Statistical properties of experimental coherent waves in microcavity lasers: Analogous study of quantum billiard wave functions

C. C. Chen, C. C. Liu,* K. W. Su, T. H. Lu, Y. F. Chen, and K. F. Huang
Department of Electrophysics, National Chiao Tung University, 1001 Ta Hsueh Road, Hsinchu, 30050 Taiwan, Republic of China
(Received 5 November 2006; revised manuscript received 10 January 2007; published 2 April 2007)

We use a microcavity laser to explore the properties of experimental coherent waves as an analogous study of the chaotic wave functions in quantum billiards. With the eigenstate expansion method, the experimental high-order chaotic coherent waves are well reconstructed. The reconstructed wave functions are employed to calculate the field and intensity correlations. It is found that the spreading of *k*-space (momentum space) distribution leads to not only wave localization in coordinate space but also enhancement of long-range correlations.

DOI: 10.1103/PhysRevE.75.046202 PACS number(s): 05.45.Mt, 03.65.Ge, 42.55.Sa, 42.60.Jf

I. INTRODUCTION

Quantum billiards as paradigm models are often used to examine the quantum chaotic properties corresponding to classical chaotic systems. Most theoretical studies of quantum billiard problems are concentrated on energy-level statistical features [1–4]. For chaotic wave functions, Berry conjectured that the higher eigenmodes of a ray-chaotic Hamiltonian should be statistically indistinguishable from a superposition of plane waves of fixed wave-vector magnitude with random amplitude, phase, and direction [5]. He showed that the space-averaged spatial correlation of the two-dimensional wave function is given by a Bessel function of zeroth order. The conjecture has attracted many theoretical studies with satisfactory results [1–4]. However, on the experimental side, besides resonance energies, the wave functions are also interfered with in the measuring processes [6,7]. For example, the microwave cavity is perturbed by a metallic bead [8–10], the quantum dot is interacted with the tip of an atomic force microscope [11], and the microcavity laser is externally driven to be oscillating and raying [12,13].

It is known that microwave cavities have been used mostly in experimental analogized studies of quantum billiards, in which the statistics of wave function imagings has been obtained successfully [9,10]. Recently, it has been also reported that with microcavity lasers the transverse-mode patterns can be analogously interpreted as the wave function imagings of quantum billiards [12,13]. The coherent wave in laser cavities enables one to achieve precise measurements of intensity patterns. Nevertheless, the work of transforming the intensity patterns into field distributions for the purpose of getting more information from the wave functions has never been realized so far in microcavity lasers.

In this paper, we fabricate chaotic-shaped oxide-confined vertical cavity surface emitting lasers (VCSELs) with a large aperture and measure the near-field transverse patterns. We reconstruct the wave functions of these coherent optical chaotic patterns by judging the signs of the nodal domains [14,15] and exploiting the orthogonality integrals of Fourier series. We find that the reconstructed wave function is composed of a set of nearly degenerate wave vectors k, which are spreading on a ring area to a certain extent. By using these wave functions we explore the statistical properties of the experimental chaotic optical transverse patterns of microcavity as an analogous study of the chaotic wave function in quantum billiards. We also study the statistical characteristics of the wave functions with localizations on the periodic orbits in the square billiard for comparison.

II. EXPERIMENTAL RESULTS

The VCSEL cavity with a large aperture can be interpreted as a two-dimensional billiard (microcavity) because of large index discontinuities between the oxide layer and surrounding semiconductor material [12,13]. The device structure of these oxide-confined VCSELs is similar to that described in Ref. [12]. The size of our oxide aperture is $40 \times 40\ \mu m^2$, and the effective cavity length between two distributed feedback reflectors is designed to have an emission wavelength around 808 nm (a single longitudinal frequency because of the short cavity length). The near-field patterns are measured with a (340×280)-pixel charge-coupled-device (CCD) camera (Coherent, Beam-Code) and an optical setup similar to Ref. [12]. An optical spectrum analyzer (ADVANTEST Q8347) is used to monitor the spectral information of the laser with a resolution of 0.002 nm. Comparing to the transverse-mode spacing $\Delta\lambda_t \approx \lambda_z^3/(4a^2) = 0.0824$ nm, the transverse-mode spectral information can be clearly resolved.

We cooled the device to a temperature around 260 K. Near the lasing threshold the transverse pattern is emitted from the VCSEL device. Experimental results show that the transverse patterns of square-shaped cavities can be evidently divided into two regimes of low-divergence and high-divergence emissions. It is expected that the thermal-lensing effect will switch the device into the low-divergence regime because the joule heating induces a rising temperature across the device cross section. Typically, high-divergence patterns are very symmetric and those of the low divergence are more irregular. Therefore, it is easy to differentiate the regimes in which the lasers are operated. On the other hand, the transverse patterns emitted from deformed-square-shaped cavi-

*Electronic address: ccliu@cc.nctu.edu.tw

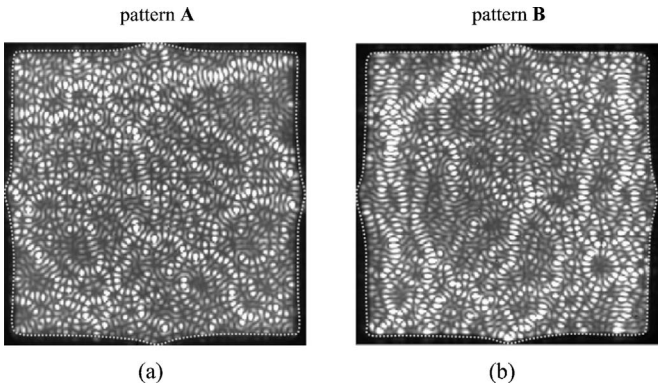

FIG. 1. The near-field patterns of the same shaped device with a moderate ripple boundary deformed from square (size of the oxide aperture is 40×40 μm^2): (a) pattern A and (b) pattern B, where white color represents the highest value of intensity in the gray level. The dashed lines are depicted to indicate the boundaries of the cavities.

ties, in the shape of a moderate ripple, are found to be linearly polarized and always ergodic.

The photons inside the microcavity laser are reflected by and oscillated between the two mirrors (z direction), which are designed to be a high reflection rate (about 99.9%). Inside the cavity, in the transverse (xy) direction the photons behave as standing waves confined by the oxide aperture. In the longitudinal (z) direction they oscillate between the two plane mirrors also forming standing waves. After separating the z component in the wave equation, we are left with a two-dimensional Helmholtz eqution $(\nabla_t^2+k_t^2)\psi(x,y)=0$. The wave functions inside the cavity can be expressed as standing waves: $\Psi^{\text{in}}(x,y,z)=\psi(x,y)\sin k_z z$. The section wave patterns at different $z=z_i$ positions inside the cavity are almost identical with only a difference of factor of $|\sin k_z z_i|^2$ between their intensities. Once the photon is emitted out of the cavity in the z direction, the information of $\psi(x,y)$ can be carried out by the longitudinal wave vector k_z and the wave function will then become $\Psi^{\text{out}}(x,y,z)=\psi(x,y)\exp(-ik_z z)$. The near field of the microcavity laser is the field at the starting emission plane ($z=0$) out of the cavity and equivalent to the field of the xy plane inside the cavity.

Figure 1 shows two near-field patterns of the microcavity lasers, denoted as pattern A and pattern B, with the same deformed-square-shaped cavity. The boundary of the cavity is in the shape of a moderate ripple, which is depicted by the dashed line. These two patterns have very clear formations including nodal lines and nodal domains. The optical spectrum for the laser beam reveals that the linearly polarized transverse pattern is a single-frequency oscillation; namely, it is a stationary state. Previous laser experiments have proved that the transverse-mode locking is an important process in transverse pattern formation [6,16,17].

III. NUMERICAL ANALYSIS AND DISCUSSION

Since the experimental patterns captured by the CCD camera are in the form of intensity point matrices $|\psi(x_i,y_j)|^2$,

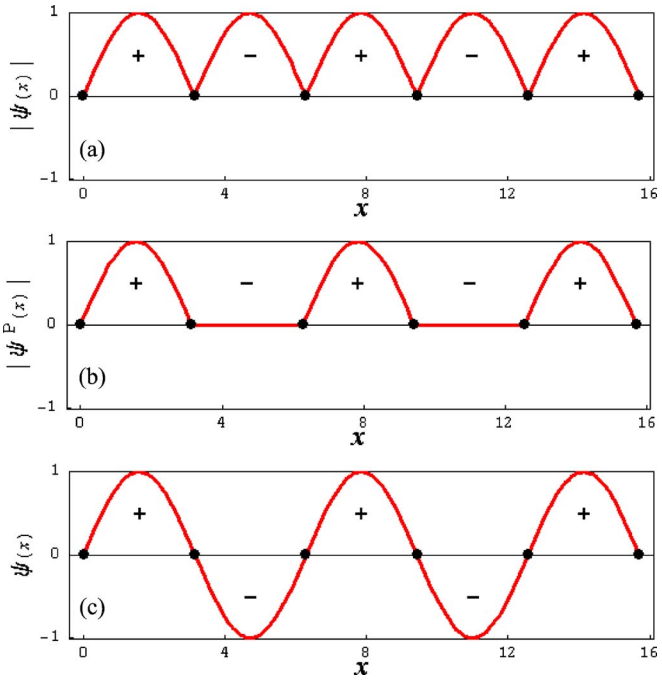

FIG. 2. (Color online) The one-dimensional sine wave function $\psi(x)$ can be obtained from its absolute wave function $|\psi(x)|$ and positive wave function $|\psi^P(x)|$ by the equation of $\psi(x)=2|\psi^P(x)|-|\psi(x)|$. The ⌜●⌟ are the nodal points and the positive (negative) domains are marked by + (−).

which are always positive, we will need to reconstruct the wave functions for further statistical analysis. However, the wave field cannot be obtained from $|\psi(x_i,y_j)|^2$ by just taking the square root as it is only related to its magnitude. Here the indices of i and j ($i,j=1,2,\ldots,S$) denote the positions in the pattern, where S is determined by the position resolution of the CCD camera and the image size of the pattern; the intensity data we obtained are a $S\times S=200\times200$ matrix.

To obtain the wave function, the first step is to translate the intensity point matrix $|\psi(x_i,y_j)|^2$ into the field point matrix $\psi(x_i,y_j)$. According to Blum *et al.* [14] and Bogomolny and Schmit [15], the positive and negative nodal domains of the wave function can be separated by the nodal lines [in which $\psi(x_i,y_j)=0$]. Therefore, the field point matrix $\psi(x_i,y_j)$ can be constructed from the intensity point matrix $|\psi(x_i,y_j)|^2$ by taking the square root and judging the signs of the nodal domains. As an illustration in Fig. 2, the nodal points ⌜●⌟ separate the positive and negative domains of the absolute sine wave function $|\psi(x)|$, marked by "+" and "−." The positive wave function $|\psi^P(x)|$ is obtained by setting the negative domains of the absolution wave function $|\psi(x)|$ to be zero. The one-dimensional sine wave can be obtained by

$$\psi(x)=2|\psi^P(x)|-|\psi(x)|. \tag{1}$$

Similarly, the two-dimensional positive wave functions can be obtained by judging the signs of the nodal domains that are separated by the nodal lines and setting the negative ones to be zero. In Figs. 3(a) and 3(b), we show the density plots of $|\psi^P(x_i,y_j)|$ for pattern A and pattern B, respectively. With

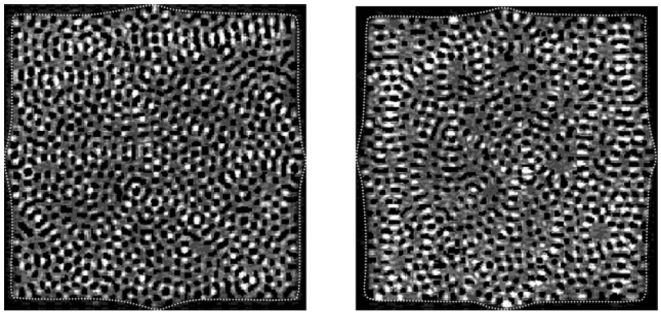

FIG. 3. The intensity plots of the positive wave functions $|\psi^{p}(x,y)|$ of pattern A (a) and pattern B (b). The dashed lines are depicted to indicate the boundaries of the cavities.

the equation of $\psi(x_i,y_j)=2|\psi^{p}(x_i,y_i)|-|\psi(x_i,y_i)|$, their field point matrices are derived.

Except for the restriction of the position resolution $(S\times S)$, the intensity resolution of patterns is discrete to 8 levels, while it is multiplied to 15 levels for the wave field. The discontinuousness make the pattern information from the experiment not precise enough for the study. So one will need to reconstruct the wave function $\psi(x,y)$ from the field point matrix $\psi(x_i,y_j)$ as the second step. Since the Helmholtz equation $(\nabla^2+k^2)\psi=0$ can be viewed as the time-independent Schrödinger equation for the motion of a particle (with a mass) [12,13,18], the eigenfunctions of a square rigid boundary (square billiard) can be given by

$$\psi_{m,n}(x,y)=\frac{2}{a}\sin\frac{m\pi x}{a}\sin\frac{n\pi y}{a}, \tag{2}$$

with the wave numbers being

$$k_{mn}^2=k_x^2+k_y^2=\left(\frac{m\pi}{a}\right)^2+\left(\frac{n\pi}{a}\right)^2, \tag{3}$$

where a is the billiard length and m (n) is the quantized number in the x (y) direction. Note that the energy here is proportional to k for a photonic wave, while the energy for a material wave is proportional to k^2. With the eigenstate expansion method, the two-dimensional coherent wave functions of the weakly deformed-square billiard can be represented by a double Fourier sine series

$$\psi(x,y)=\sum_{m=1}^{\infty}\sum_{n=1}^{\infty}A_{mn}\frac{2}{a}\sin\frac{m\pi x}{a}\sin\frac{n\pi y}{a}, \tag{4}$$

where the coefficients A_{mn} can be obtained by the orthogonality relations

$$A_{mn}=\frac{2}{a}\int_0^a\int_0^a\psi(x,y)\sin\frac{m\pi x}{a}\sin\frac{n\pi y}{a}dxdy. \tag{5}$$

For the separate points (x_i,y_j), the continuing integral would be transformed into a summation form with the field point matrix $\psi(x_i,y_j)$:

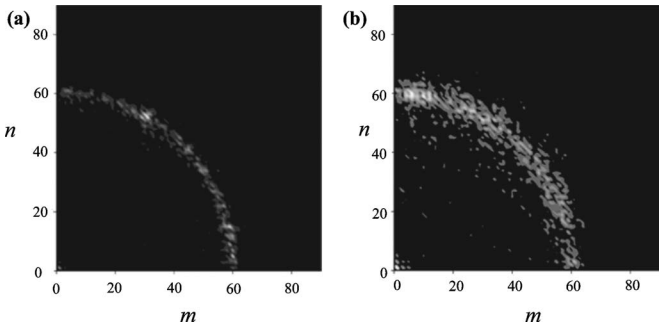

FIG. 4. Distribution of the coefficients $|A_{mn}|$ obtained by Fourier analysis in Eq. (6) for the patterns in Fig. 1: (a) $|A_{mn}|$ of pattern A and (b) $|A_{mn}|$ of pattern B.

$$A_{mn}=\frac{2}{a}\sum_{i=1}^{S}\sum_{j=1}^{S}\psi(x_i,y_j)\sin\frac{m\pi x_i}{a}\sin\frac{n\pi y_j}{a}\Delta x_i\Delta y_j. \tag{6}$$

Our method is similar to the study of the deformed half-circular microwave rough billiard in Ref. [19].

Figure 4 depicts the magnitude of the coefficient $|A_{mn}|$ for pattern A and pattern B in Figs. 1(a) and 1(b), respectively, in which white color represents the highest value of $|A_{mn}|$ in the gray level. Figure 4 can be looked as the momentum-space representation of the wave functions, since $(p_x,p_y)\propto(k_x,k_y)=\frac{\pi}{a}(m,n)$. As mentioned in Ref. [13], Fig. 4 would also be the far-field intensity in the optical phenomenon, because the far-field intensity is essentially the spatial two-dimensional Fourier transform of the near-field pattern. The distribution of $|A_{mn}|$ in Fig. 4(a) is concentrated on a smaller ring area with the mean value $\bar{k}^A=60.92\pi/a$ and standard deviation $\sigma_k^A=1.35\pi/a$, while $|A_{mn}|$ in Fig. 4(b) is spreading on a wider area with $\bar{k}^B=60.14\pi/a$ and $\sigma_k^B=1.62\pi/a$. Here we have calculated the mean value and standard deviation of k by $\bar{k}=\Sigma_{m,n}A_{mn}^2k_{mn}$ and $\sigma_k=[\Sigma_{m,n}A_{mn}^2(k_{mn}-\bar{k})^2]^{1/2}$ with $\Sigma_{m,n}A_{mn}^2=1$. These ring areas signify the random directional distributions of the wave vectors $\boldsymbol{k}$. In contrast with the chaotic wave function, the k-space distribution of the wave function with localization on the periodic orbit is further focused on the disk area on the ring [13].

Strictly speaking, the coherent wave function obtained from Eq. (4) is not a stationary state because the eigenstate components are not exactly degenerate for the Hamiltonian H. Nevertheless, the results shown in Fig. 4 demonstrate that the dominative eigenstates for patterns A and B are nearly degenerate. In other words, as dominative eigenstates satisfy $\Delta H/\langle H\rangle\to 0$—i.e., $\sigma_k\to 0$ from the distribution of $|A_{mn}|$ associated with k_{mn} in Eq. (3)—the wave function in Eq. (4) is guaranteed to be a stationary state in the classical limit. Hence, the distribution of $|A_{mn}|$ is associated with the constraint of the minimum-energy uncertainty.

The reconstructed coherent optical wave functions $\psi(x,y)$ are obtained by substituting the coefficients A_{mn} into Eq. (3), which are shown in Figs. 5(a) and 5(b) for pattern A and pattern B in Figs. 1(a) and 1(b), with the indices m and n

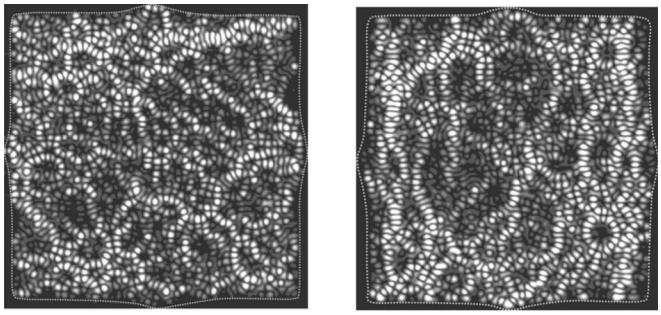

(a) (b)

FIG. 5. Density plots of reconstructed coherent optical wave functions obtained by Eq. (4) with A_{mn} from Eq. (6) for (a) pattern A and (b) pattern B in Fig. 1 with indices m and n being summed up from 1 to 90. The dashed lines are depicted to indicate the boundaries of the cavities.

being summed up from 1 to 90, respectively. It is very successful in reconstructing the experimentally observed patterns such that one will be very hard to distinguish the difference between Figs. 1 and 5.

The participating eigenstates and their weights as in Eq. (4) determine the appearance and stability of the experimental near-field patterns. As stated above, the k-space distributions in Fig. 4 suggest to us that the eigenstates contributing to the experimental pattern are concentrated on a ring, nearly degenerate to a single frequency. In other words, the number of the dominative states for the wave function is rather small compared to the entire range of k space ($m=1,\ldots,90,\ldots$ and $n=1,\ldots,90,\ldots$). It is intriguing that if we reduce the number of superposing eigenstates for the reconstructed wave functions, the density plots will still look similar. As an instance, if we choose eigenstates with higher values of $|A_{mn}|$, 327 (411) eigenstates for pattern A (pattern B), to reconstruct wave functions, most pattern information is still retained. The smaller the magnitude of σ_k is, the fewer the dominant eigenstates of the reconstructed wave function will be. As discussed in previous studies [20,21], the wave function obtained as a superposition of a few nearly degenerate eigenstates may provide a more physical description of phenomena than the true eigenstates in real mesoscopic systems. The experimental results also show that the selection of the nearly degenerate eigenstates is as the process of transverse mode locking, which makes the wave functions have the minimum-mode volume for the lowest lasing threshold.

The statistical properties of the chaotic behavior of the measured wave functions can be studied by evaluating the amplitude and intensity distributions and the spatial correlations. According to the Berry conjecture, the chaotic wave functions in a billiard should be statistically indistinguishable from a superposition of plane waves of fixed wave-vector magnitude with random amplitude, phase, and direction [5]. As an immediate consequence of the central limit theorem one obtains chaotic waves in the form of a Gaussian distribution for the amplitude [1–4],

$$P(\psi) = \frac{1}{\sigma\sqrt{2\pi}} \exp(-\psi^2/2\sigma^2), \tag{7}$$

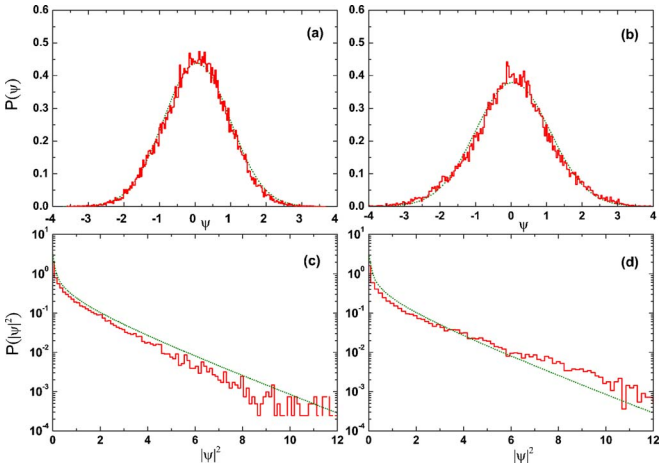

FIG. 6. (Color online) Statistical features of the reconstructed coherent optical wave functions for experimental pattern A and pattern B in Fig. 1 with the amplitude [intensity] distributions (solid step line) compared to the Gaussian [Porter-Thomas] distributions (dashed line) with (a) $\sigma=0.92$ and (b) $\sigma=1.05$.

where σ is the standard deviation and the form of the Porter-Thomas distribution for the intensity reads

$$P(|\psi|^2) = \frac{1}{\sqrt{2\pi|\psi|^2}} \exp(-|\psi|^2/2). \tag{8}$$

The amplitude distributions of the reconstructed wave functions are illustrated in Figs. 6(a) and 6(b), and their intensity distributions are shown in Figs. 6(c) and 6(d) for experimental pattern A and pattern B, respectively, where the dashed lines are the theoretical expectations. The amplitude distribution of the reconstructed pattern A in Fig. 6(a) compared to that of pattern B in Fig. 6(b) is more fitted to the Gaussian line, because of its smaller standard deviation σ_k. Similarly, the intensity distribution in Figs. 6(c) and 6(d) has the same phenomenon.

The definitions for field and intensity correlations are given as [5]

$$F(r) = \langle \psi(\mathbf{x})\psi(\mathbf{x}+\mathbf{r})\rangle, \tag{9}$$

$$I(r) = \langle |\psi(\mathbf{x})|^2 |\psi(\mathbf{x}+\mathbf{r})|^2\rangle, \tag{10}$$

where the angular brackets $\langle\ \rangle$ represent spatial average over the position $\mathbf{x}=(x,y)$ and the direction of the vector $\mathbf{r}$, and $r=|\mathbf{r}|$ is the separation distance. Figure 7 shows the correlations of the field in (a) and (b) and the intensity in (c) and (d) for reconstructed pattern A and pattern B in Fig. 5 compared to the theoretical expectations. As the wave functions have been normalized with $\langle[\psi(\mathbf{x})]^2\rangle=1$, the *inverse participation ratios* (IPRs), defined by $I_2=\langle[\psi(x)]^4\rangle$ [10,22], are obtained to be 3.238 and 3.385 for pattern A and pattern B, respectively. For chaotic systems the IPRs can be immediately obtained from a Porter-Thomas distribution—i.e., IPR $=\int_0^\infty I^2 P_{\mathrm{PT}}(I)dI=3.0$, which is a universal value. Based on the Berry conjecture, for a high-order chaotic wave function, the field correlation is $J_0(k_f r)$, and its intensity correlation is $1+2J_0^2(k_f r)$. Here k_f is the fixed (governing) wave number and

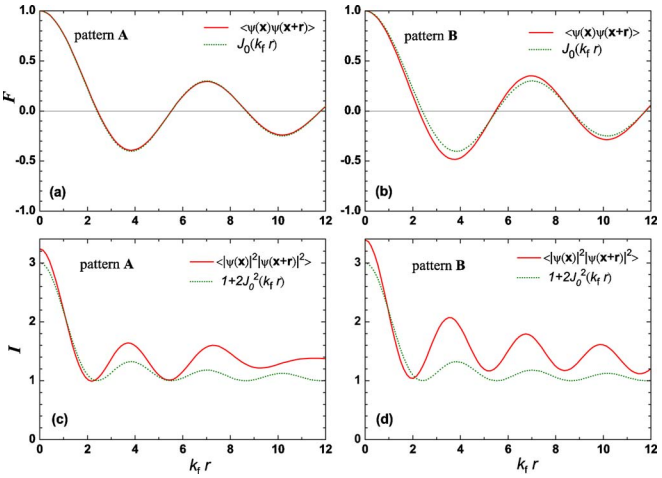

FIG. 7. (Color online) Correlations of the fields in (a) and (b) and intensity in (c) and (d) for pattern A and pattern B, respectively. The dashed lines represent the theoretical values and the solid lines are the correlations computing from the reconstructed coherent optical wave functions as shown in Fig. 3.

we substitute it by the mean wave numbers $\bar{k}^A_{mn}=60.92\pi/a$ and $\bar{k}^B_{mn}=60.14\pi/a$ for pattern A and pattern B, respectively.

Microwave cavities have been manifested statistical results that show very good agreement with the Berry conjecture in chaotic billiards [10]. However, the inadequacy of the conjecture occurs in some other experimental systems as they are more complicated than the scalar billiard [23–25]. For example, in the aluminum plate [23] one has to consider the longitudinal and transverse wave vectors because of the plate thickness, and in the multimode fiber [24] the correlation is contributed by multifrequencies. The former depicts the average intensity correlation from several intensity measurements of in-plane standing waves, while the latter obtains results in the field correlation from its far-field intensity. Our statistical results are not fitted to the theoretical conjecture either. The most important reason is that the existence of the standard deviation σ_k, the width of the nearly degenerated modes in experiments, causes a deviation from the theoretical line. Especially, in pattern B the field correlation is slightly deviant, while the intensity correlation represents a large deviation. The intensity correlation is no more than $1+2[\Sigma_{m,n}A^2_{mn}J_0(k_{mn}r)]^2=1+2J^2_0(k_f r)$, but one has to consider the contribution of the interference between different participating eigenstates.

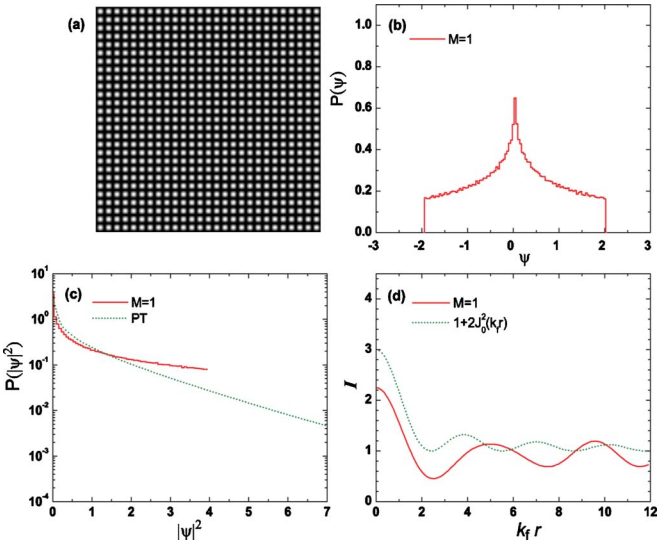

FIG. 8. (Color online) The partial coherent state with $N=52$, $M=1$, and $\phi=\pi/2$: (a) density plot, (b) amplitude distribution, (c) intensity distribution, and (d) intensity correlation.

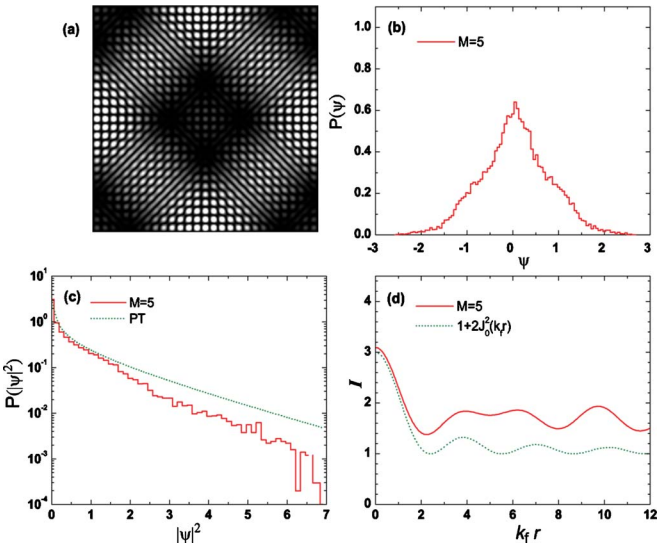

FIG. 9. (Color online) Same as Fig. 8 but for $M=5$.

On the other hand, we may also compare the above statistical characteristics to that of the wave functions in the square billiard. According to Refs. [13,20], wave functions with localizations on the high-order periodic orbits can be expressed by the partially coherent states

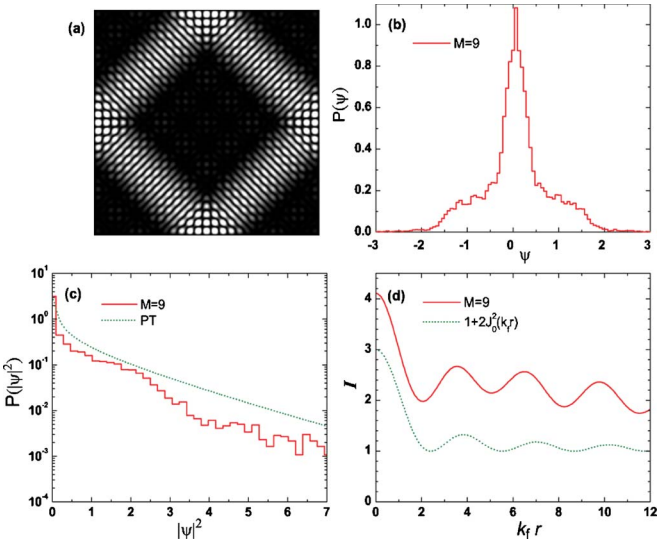

FIG. 10. (Color online) Same as Fig. 8 but for $M=9$.

$$\psi_{N,M}^{\cos}(x,y;\phi) = \frac{(2/a)}{\left[\sum_{K=J}^{N-J}\binom{N}{K}\cos^2 K\phi\right]^{1/2}} \times \sum_{K=J}^{N-J}\binom{N}{K}^{1/2}(\cos K\phi)\sin\left[(K+1)\frac{\pi x}{a}\right] \times \sin\left[(N-K+1)\frac{\pi y}{a}\right], \quad (11)$$

where N is the order of the states, ϕ is related to the wall positions of specular reflection points, and the index $M=N-2J+1$ represents the number of eigenstates used in the wave function. We show the density plots and statistical results for $N=52$, $\phi=\pi/2$, and $M=1$, 5, and 9 in Figs. 8–10, respectively. The mean values and standard deviations of the wave numbers are $\bar{k}=38.18\pi/a$, $38.25\pi/a$, and $38.35\pi/a$ and $\sigma_k=0$, $0.050\pi/a$, and $0.164\pi/a$, respectively. Their characteristics of the amplitude distributions, intensity distributions, and intensity correlations of these wave functions are all dissimilar and also different from those in chaotic wave functions, while the field correlations are all very near the Bessel function as well as that of the chaotic systems, among which the case of $M=1$ is composed of only a single eigenstate, which is equal to Eq. (2) with $m=26$ and $n=26$. The cases of $5\leqslant M\leqslant 9$ have been verified in Ref. [20] that their density distributions coincide with the experimentally observed patterns. The IPR values for the wave patterns in Figs. 8(a), 9(a), and 10(a) are 2.250, 3.097, and 4.113, respectively. The intensity correlation can be compared with the result of $1+2J_0^2(k_f r)$ to identify the extra contribution to be the long-range correlation. It can be found that wave functions with broader spreading of wave vector distributions (larger σ_k) will get a higher IPR and higher contribution from long-range correlation as well as the chaotic cases in Fig. 7. A similar phenomenon can be also observed in the transmission of microwaves and light in random media [26,27].

IV. CONCLUSION

In summary, we have successfully used a microcavity laser to perform an analogous study of the chaotic wave functions in quantum billiards. To explore the experimental coherent waves, high-order chaotic optical waves have been well reconstructed with the eigenstate expansion method and used to study the statistical properties. It has been found that the amplitudes of the experimental high-order chaotic patterns behavior like a Gaussian distribution and their intensities obey the Porter-Thomas distribution. Moreover, we have found that the spreading of the k-space distribution of a coherent optical wave function, in both chaotic and square billiards, results in not only a spatial localization but also an enhancement of its long-range intensity correlation.

ACKNOWLEDGMENTS

This work was supported in part by the MOE-ATU project and the National Science Council under Contract No. NSC-95-2112-M-009-041-MY2.

[1] M. C. Gutzwiller, *Chaos in Classical and Quantum Mechanics* (Springer-Verlag, New York, 1990), and references cited therein.
[2] H. J. Stöckmann, *Quantum Chaos: An Introduction* (Cambridge University Press, Cambridge, U.K., 1999), and references cited therein.
[3] T. Guhr, A. Müller-Groeling, and H. A. Weidenmüller, Phys. Rep. **299**, 189 (1998), and references cited therein.
[4] P. Šeba, Phys. Rev. Lett. **64**, 1855 (1990); F. Borgonovi, G. Casati, and B. Li, *ibid.* **77**, 4744 (1996); K. M. Frahm and D. L. Shepelyansky, *ibid.* **78**, 1440 (1997); O. Bengtsson, J. Larsson, and K. F. Berggren, Phys. Rev. E **71**, 056206 (2005).
[5] M. V. Berry, J. Phys. A **10**, 2083 (1977); P. O'Connor, J. Gehlen, and E. J. Heller, Phys. Rev. Lett. **58**, 1296 (1987); S. W. McDonald and A. N. Kaufman, Phys. Rev. A **37**, 3067 (1988).
[6] J. Scheuler and M. Orenstein, Science **285**, 230 (1999).
[7] M. Mendoza and P. A. Schulz, Phys. Rev. B **74**, 035304 (2006); R. G. Nazmitdinov, K. N. Pichugin, I. Rotter, and P. Šeba, *ibid.* **66**, 085322 (2002).
[8] H.-J. Stöckmann and J. Stein, Phys. Rev. Lett. **64**, 2215 (1990); J. Stein and H.-J. Stöckmann, *ibid.* **68**, 2867 (1992); H.-D. Gräf, H. L. Harney, H. Lengeler, C. H. Lewenkopf, C. Rangacharyulu, A. Richter, P. Schardt, and H. A. Weidenmüller, *ibid.* **69**, 1296 (1992); H. Alt, H. D. Gräf, H. L. Harney, R. Hofferbert, H. Lengeler, A. Richter, P. Schardt, and H. A. Weidenmüller, *ibid.* **74**, 62 (1995).
[9] S. Sridhar, Phys. Rev. Lett. **67**, 785 (1991).
[10] A. Kudrolli, V. Kidambi, and S. Sridhar, Phys. Rev. Lett. **75**, 822 (1995); P. Pradhan and S. Sridhar, *ibid.* **85**, 2360 (2000).
[11] M. A. Topinka, B. J. LeRoy, S. E. J. Shaw, E. J. Heller, R. M. Westervelt, K. D. Maranowski, and A. C. Cossard, Science **289**, 2323 (2000); R. Crook, C. G. Smith, A. C. Graham, I. Farrer, H. E. Beere, and D. A. Ritchie, Phys. Rev. Lett. **91**, 246803 (2003).
[12] S. P. Hegarty, G. Huyet, J. G. McInerney, and K. D. Choquette, Phys. Rev. Lett. **82**, 1434 (1999).
[13] K. F. Huang, Y. F. Chen, H. C. Lai, and Y. P. Lan, Phys. Rev. Lett. **89**, 224102 (2002).
[14] G. Blum, S. Gnutzmann, and U. Smilansky, Phys. Rev. Lett. **88**, 114101 (2002).
[15] E. Bogomolny and C. Schmit, Phys. Rev. Lett. **88**, 114102 (2002).
[16] L. A. Lugiato, C. Oldano, and L. M. Narducci, J. Opt. Soc. Am. B **5**, 879 (1988).
[17] Y. F. Chen and Y. P. Lan, Phys. Rev. A **64**, 063807 (2001); Y. F. Chen and Y. P. Lan, *ibid.* **65**, 013802 (2002).
[18] J. J. Hupert and G. Ott, Am. J. Phys. **34**, 260 (1966).

[19] N. Savytskyy, O. Hul, and L. Sirko, Phys. Rev. E **70**, 056209 (2004).
[20] Y. F. Chen, K. F. Huang, and Y. P. Lan, Phys. Rev. E **66**, 046215 (2002).
[21] R. Narevich, R. E. Prange, and O. Zaitsev, Phys. Rev. E **62**, 2046 (2000); W. Li, L. E. Reichl, and B. Wu, *ibid.* **65**, 056220 (2002).
[22] Y. V. Fyodorov and A. D. Mirlin, Phys. Rev. B **51**, 13403 (1995).
[23] K. Schaadt, T. Guhr, C. Ellegaard, and M. Oxborrow, Phys. Rev. E **68**, 036205 (2003).
[24] V. Doya, O. Legrand, F. Mortessagne, and C. Miniatura, Phys. Rev. Lett. **88**, 014102 (2002); Phys. Rev. E **65**, 056223 (2002).
[25] A. Akolzin and R. L. Weaver, Phys. Rev. E **70**, 046212 (2004).
[26] P. Sebbah, B. Hu, A. Z. Genack, R. Pnini, and B. Shapiro, Phys. Rev. Lett. **88**, 123901 (2002).
[27] Y. F. Chen, K. W. Su, T. H. Lu, and K. F. Huang, Phys. Rev. Lett. **96**, 033905 (2006); S. H. Chang, A. Taflove, A. Yamilov, A. Burin, and H. Cao, Opt. Lett. **29**, 917 (2004).